Disordered to ordered phase transformation: Correlation between microstructure and magnetic properties in Fe-Pd thin films

Journal of Applied Physics

RESEARCH ARTICLE | MARCH 30 2022

Disordered to ordered phase transformation: Correlation between microstructure and magnetic properties in Fe–Pd thin films

S. Bahamida; A. Fnidiki ; M. Coïsson ; E. S. Olivetti ; G. Barrera ; F. Celegato; P. Tiberto; M. Boudissa

Journal of Applied Physics 131, 123902 (2022)
https://doi.org/10.1063/5.0085898

Journal of Applied Physics ARTICLE scitation.org/journal/jap

Disordered to ordered phase transformation: Correlation between microstructure and magnetic properties in Fe–Pd thin films

Cite as: J. Appl. Phys. **131**, 123902 (2022); doi: 10.1063/5.0085898
Submitted: 20 January 2022 · Accepted: 14 March 2022 ·
Published Online: 30 March 2022

S. Bahamida,[1,2] A. Fnidiki,[3] M. Coïsson,[4,a)] E. S. Olivetti,[4] G. Barrera,[4] F. Celegato,[4] P. Tiberto,[4] and M. Boudissa[5]

AFFILIATIONS

[1]Research Unit, Materials, Processes and Environment (RU/MPE), University of M'Hamed Bougara, 1 Avenue de l'Independance, Boumerdes 35000, Algeria
[2]Physics Department, Faculty of Sciences, University of M'Hamed Bougara Boumerdes, 35000 Boumerdes, Algeria
[3]Groupe de Physique des Matériaux, Université et INSA de Rouen—UMR CNRS 6634—Normandie Université, F-76801 Saint Etienne du Rouvray, France
[4]Advanced Materials and Life Sciences Division, INRIM, Strada delle Cacce 91, 10135 Torino (TO), Italy
[5]ENMC Laboratory, Department of Physics, Faculty of Sciences, University Ferhat Abbas, Setif 19000, Algeria

[a)]**Author to whom correspondence should be addressed:** m.coisson@inrim.it

ABSTRACT

The kinetics of the transformation from the disordered to the ordered phase has been studied in $Fe_{56}Pd_{44}$ thin films deposited on silicon substrates by Joule evaporation. Subsequent thermal treatments at 550 °C in vacuum were performed at different annealing times to promote the formation and the optimization of the ordered $L1_0$ FePd phase. X-ray diffraction allowed us to investigate the microstructure of the samples (grain size, volume fraction of the transformed phase, order parameter of the ordered phase, and average order of the alloy), whereas magnetic measurements allowed us to evaluate coercivity and to independently estimate the volume fraction of the ordered $L1_0$ phase. The kinetics of the transformation turned out to reach completion after 20 min of annealing time with the grain size growing with a power law with an exponent equal to 8.24. The resulting monophasic film has a high density of defects, which contribute to the magnetic coercivity. A linear relationship between the coercive field and the average order parameter of the alloy has been established. Finally, the evolution of the transformed phase obeys Avrami's law with an exponent of ∼0.4, indicating that the transformation is controlled by the nucleation mechanism without grain growth.

I. INTRODUCTION

$L1_0$ ordered ferromagnetic intermetallics, such as FePt, FePd, and CoPt, are of technological interest due to their large uniaxial magneto-crystalline anisotropy (K_u, 6.6×10^7 erg/cm^3 for FePt, 1.8×10^7 erg/cm^3 for FePd, and 9.4×10^7 erg/cm^3 for CoPt),[1] which confers them a high coercive field. However, the details of the microstructure of these materials turn out to affect coercivity in a complex way, involving the presence of the equiatomic disordered phase and how it transforms into the ordered one, including the development of defects such as c-axes variants, grain boundaries, antiphase boundaries (APBs), twins, and polytwins. For example, large values of coercivity have been attributed to domain-wall pinning at the interface between the ordered and the disordered phases and to the c-axes variant at the boundaries of the ordered phase.[2] The FePd system is extremely apt at studying domain-wall pinning by planar crystal defects and microstructural heterogeneities, as well as grain size effects, which contribute to an increase of the coercive field[3–6] through the presence of twins, polytwins, or stacking faults.

These defects develop during the disordered $A1 \rightarrow$ ordered $L1_0$ phase transformation through processes that can be controlled by suitable thermal treatments. These can be grouped into direct

heating of the substrate during deposition and post-deposition annealing of the as-prepared samples. For both groups, several annealing protocols have been attempted with different heating and cooling rates, annealing temperatures, and times, all of which affect the grain size and the formation of the structural defects during the disorder → order phase transformation. As a consequence, also, the magnetic properties are affected, allowing their optimization for applications in high-density recording, permanent magnets, spintronic devices, etc.

In Fe–Pd thin films, *in situ* annealing in electron microscopy has been exploited to study the role of the annealing temperature[7] and of the heating rates[8] for samples grown on single-crystal substrates such as MgO (001), inferring a slow rate of crystal growth. The magnetically hard $L1_0$ phase can develop with variants in three different space orientations,[5] which can induce twin structures. These, as well as stacking faults[6] and antiphase boundaries and twin boundaries,[9] have been shown to improve the alloy coercivity. Once induced by the thermal treatments, the disorder → order transition can be followed through physical properties such as magneto-crystalline anisotropy (which depends on the magnetic phases developing in the sample) and coercivity (which depends on magneto-crystalline anisotropy as well as the microstructural features of the sample) and through the order parameter of the ordered phase.[10,11] The kinetics of such a transformation has been modeled by the Johnson–Mehl–Avrami–Kolmogorov (JMAK) approach,[12] not only for FePd but also for FePt and CoPt systems,[2,13,14] which allows one to obtain the volume fraction of the transformed (ordered) phase as a function of the annealing time. The transformation can take place through the nucleation of new grains or through the growth (by diffusion or by accretion) of existing grains along either 1, 2, or 3 dimensions.[15,16] The grain growth follows a power law whose exponent n provides an indication of the mechanisms involved.

In turn, the grains' size affects the magnetic coercivity following a complex pattern,[17–20] where grain boundaries, density of grains with respect to the magnetic exchange length, crystalline anisotropy at the scale of the individual grain, and the single-domain/multi-domain boundary all play a role.

In this complex scenario, our paper aims at clearly identifying the links among microstructure, grain growth kinetics, and magnetic properties in $Fe_{56}Pd_{44}$ thin films. By exploiting suitable theoretical models on both microstructure and magnetic properties data, we have been able to investigate in detail the mechanism of grain growth and the transformed phase (from disordered to ordered) fraction as a function of the annealing time. Laws correlating the coercivity of the ordered and disordered phases, the transformed phase volume fraction, and the order parameters of the $L1_0$ phase and of the alloy as a whole have been found and experimentally validated.

II. EXPERIMENTAL

$Fe_{56}Pd_{44}$ thin films, with a thickness of 80 nm, were grown on polycrystalline silicon substrates by thermal evaporation. The alloy was prepared mixing elemental Fe and Pd powders of 99.99% purity in a tungsten crucible placed in a high vacuum chamber (base pressure 10^{-5} Pa). The operation pressure and applied average current were fixed to 7×10^{-4} Pa and 124 A, respectively. The chemical composition of the thin films was determined through energy dispersive x-ray analysis (EDX), with a relative error of 2% Pd, whereas their thickness was determined through scanning electron microscopy on samples mounted in cross section, with a relative error of 4%.

The alloy phase composition was studied using x-ray diffraction (XRD) in a pseudo-parallel beam configuration with a glancing angle of 1° of the x-ray beam (CoK_α radiation, $\lambda = 0.179\,030\,7$ nm) on the sample surface.

Annealing was performed in vacuum (base pressure 2×10^{-6} mbar) at a temperature of 550 °C for selected times. After the annealing, the samples were cooled to room temperature by free cooling, still in vacuum.

The magnetic properties of the as-prepared and annealed thin films were measured by Alternating Gradient Field Magnetometry (AGFM) at room temperature, with the magnetic field applied in the sample plane (maximum value 1.5 and 10 kOe for the as-deposited and annealed samples, respectively).

III. RESULTS

A. Microstructure

X-ray diffraction patterns of the studied $Fe_{56}Pd_{44}$ thin films are shown in Fig. 1 for the as-deposited sample and for those annealed at 550 °C at different annealing times. The diffractogram of the as-deposited sample shows the presence of the fundamental peaks (111) and (200) of the face-centered cubic (fcc) disordered FePd phase. In addition to the fundamental peaks, (110) superlattice line and the splitting of the (200) peak into the (200) and (002) peaks are observed for all the annealed films. The presence of the superstructure peak is a signature of the transformation of the disordered fcc FePd phase into the ordered $L1_0$ FePd phase that is under way.

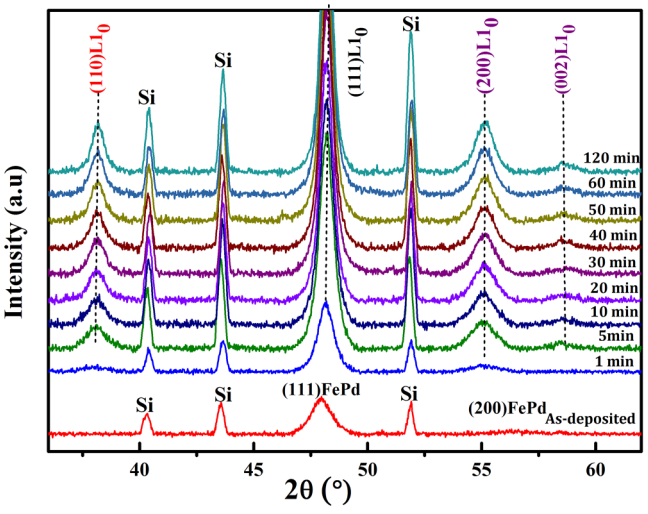

FIG. 1. X-ray diffractograms of thin $Fe_{56}Pd_{44}$ films as a function of the annealing time.

Table I summarizes the lattice constants of the fcc (disordered) and $L1_0$ (ordered) phases deduced from the x-ray diffractograms using the Bragg equation. The lattice parameter of the disordered FePd phase is calculated from the (111) peak, whereas for the ordered $L1_0$ FePd, both the (111) and the (200) peaks are taken into account. The obtained lattice constants are consistent with those reported in the literature for $L1_0$ FePd films,[21–23] being 3.82 Å < a < 3.86 Å and 3.71 Å < c < 3.75 Å. Moreover, the tetragonal ratio c/a is equal to 0.945, as expected.[24,25]

The order parameter S_{tetr} is calculated by means of the model given by Roberts,[26] which shows a good correlation with the data of different $L1_0$ phases (AuCu, CoPt),[27]

$$S_{tetr}^2 = \frac{\left(1-\frac{c}{a}\right)}{\left(1-\frac{c}{a}\right)_{S=1}}. \quad (1)$$

Table I shows the evolution of the degree of chemical ordering as a function of the annealing time. The average crystallite size <D> is calculated from the measured width of the (111) peak profile using the Scherrer equation, after subtracting the instrumental contribution to peak broadening.

B. Magnetic properties

Figure 2 shows the hysteresis loops at room temperature of the as-prepared and annealed samples, and the corresponding coercive fields as a function of the annealing time. All the hysteresis loops are measured in the in-plane configuration, except for the one shown with the magenta dashed line in Fig. 2(a), which corresponds to the sample annealed for 120 min measured with the field in the out-of-plane direction. The hysteresis loop shape of the as-deposited sample is characteristic of a soft ferromagnet, with a coercive field of 5 Oe, in agreement with XRD results that revealed the presence of only the fcc phase. Concerning the annealed samples, as the annealing time increases, the loops become wider, with typical characteristics of hard ferromagnets. A comparison of the in-plane and out-of-plane loops of the sample annealed for 120 min reveals that the transformed $L1_0$ phase grows without any preferential direction: the magnetic remanence in the in-plane configuration is still rather high, even higher than that in the out-of-plane configuration. This is compatible with a disordered distribution in space of the easy axes of the $L1_0$ crystals and is also confirmed by the Mössbauer data reported in Ref. 9. It is worth remarking that the choice of a different substrate (e.g., SiO_2 or MgO) would have probably led to a different orientation of the $L1_0$ grains and, therefore, resulted in different values of the coercivity[28] and different loop shapes, even though the kinetics of transformation discussed in the following, which should mostly depend on temperature and time, would probably have remained the same. Finally, in the case of the annealed samples, especially for the longer annealing times, a small kink in the in-plane hysteresis loops is observed close to the remanence; this kink is often attributed to the presence of a residual soft fcc phase even in the annealed samples or to defects in the hard $L1_0$ phase that determine a local magnetic softening.[29]

The coercive field monotonically increases with the annealing time [Fig. 2(b)], with an abrupt development of coercivity in the first few minutes of the thermal treatments. Initially, this is due to the transformation of the disordered fcc phase into the $L1_0$ one, followed by the appearance of structural defects (antiphase boundaries, twin boundaries, and order/disorder phase boundaries). Table I clearly shows that the disordered fcc phase completely transforms into the ordered $L1_0$ after only 10 min of heat treatment, when S_{tetr} is already equal to 1. Beyond 10 min, the coercivity continues to increase by the effect of structural defects.[9]

The coercivity is also linked to the grain size, which increases as a function of the annealing time, as illustrated in Figure 3. Different models link the coercive field H_c to the size of the grains D, such as the one by Kneller and Luborsky,[20] which accounts for

TABLE I. Structural parameters as a function of the annealing time (at 550 °C): lattice parameters of the fcc and $L1_0$ phases, average crystallite size <D>, tetragonal ratio c/a (for the $L1_0$ phase) and degree of chemical ordering s_{tetr}.

	Lattice constants (Å)					
	fcc FePd	$L1_0$ FePd		Tetragonal ratio	Degree of chemical ordering	Grain size (nm)
Annealing time (min)	$a=b=c\pm0.005$ Å	$a=b\pm0.005$ Å	$c\pm0.005$ Å	$c/a\pm0.002$	$S_{tetr}\pm0.003$	<D>
0	3.814	…	…	…	0	…
1	…	3.865	3.680	0.952	0.937	10.1
2	…	3.868	3.672	0.949	0.964	11.4
5	…	3.867	3.666	0.948	0.976	12.0
10	…	3.871	3.658	0.945	1.004	12.9
20	…	3.871	3.660	0.946	0.999	14.4
30	…	3.871	3.658	0.945	1.004	14.8
40	…	3.867	3.660	0.946	0.991	14.9
50	…	3.870	3.659	0.945	1.000	15.9
60	…	3.873	3.655	0.944	1.000	16.0
120	…	3.870	3.659	0.945	1.000	17.7

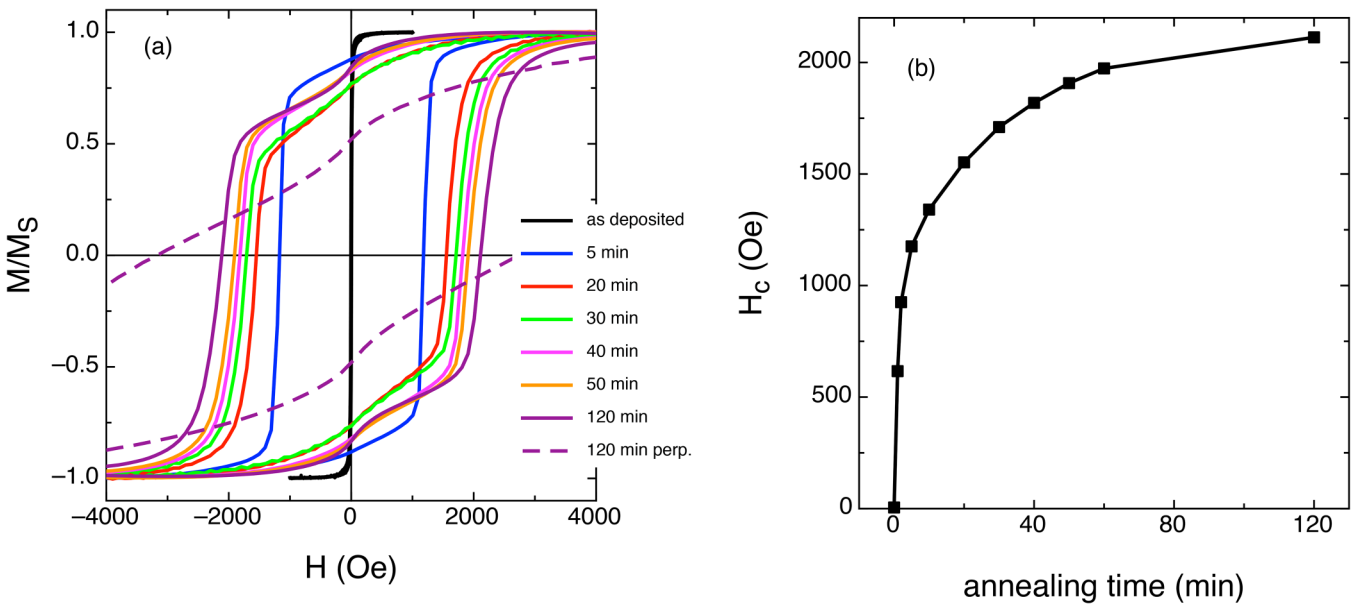

FIG. 2. (a) Selected in-plane hysteresis loops (except for the magenta dashed line, which corresponds to the out-of-plane hysteresis loop of the 120- min annealed sample) and (b) coercive field as a function of the annealing time for $Fe_{56}Pd_{44}$ thin films. The line is a guide to the eye.

an increase of H_c with $<D>$,

$$H_c = H_A\left[1 - \left(\frac{D_p}{<D>}\right)^{\frac{3}{2}}\right], \quad (2)$$

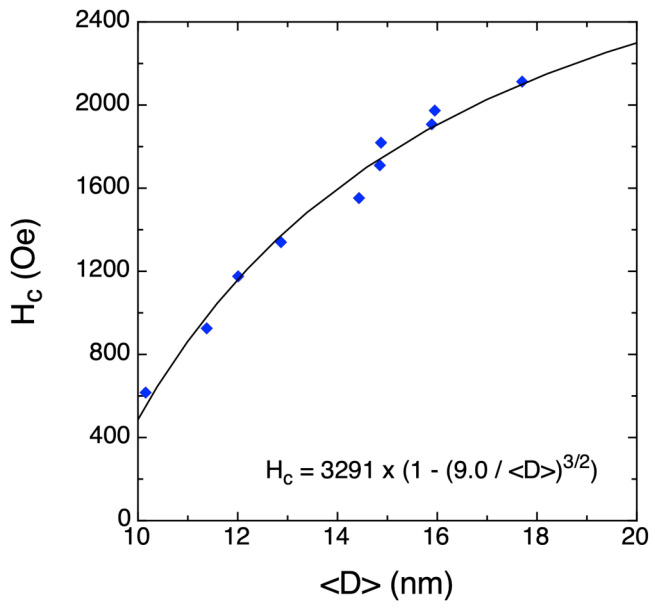

FIG. 3. Coercive field as a function of grain size.

where $H_A = 2K_1/M_S$ is the anisotropy field and D_p is the critical grain size for the transition from a superparamagnetic to a single-domain (SD) regime. Expression (2) is valid for an assembly of randomly oriented non-interacting SD particles with $D_p \ll D_{MD}$, where D_{MD} is the critical size for a transition from a single-domain to a multiple-domain regime. D_p and D_{MD} of FePd are theoretically calculated and are in the range of 5–40 nm.[1] The experimental data in Fig. 3 are fitted with Eq. (2), giving $H_A^{fit} = 3291$ Oe and $D_p^{fit} = 9.0$ nm. For our samples, the grains are, therefore, all the time above the superparamagnetic limit, as expected. Thus, the magnetic structure present in the $Fe_{56}Pd_{44}$ thin film is characterized by weakly exchange-coupled SD grains. This is deduced for the case of the FePt thin films.[14] On the other hand, the obtained value of the anisotropy field H_A^{fit} is reduced by a factor of 10 compared with the theoretical value $H_A^{th} = 33\,000$ Oe,[1] obtained assuming $H_A^{th} = 2K_1/M_S$, $K_1 = 1.8 \times 10^7$ erg/m^3, and $M_S = 1100$ emu/cm^3.[1] This reduction is similar to that obtained in the FePt systems,[14] where it was attributed to local compositional fluctuations, structural defects, and the misorientation of the anisotropy axis from grain to grain. In our present study, we also attribute this reduction to the presence of structural defects.[9]

IV. DETERMINATION OF THE TRANSFORMED PHASE FRACTION

A. From microstructure data

In order to calculate the transformed phase volume fraction from XRD data, a relationship between the order parameter and the volume fraction of the $L1_0$ phase is devised. It is useful to remind here that the departure from a perfect order in a binary superlattice

can be described by the long-range order parameter S, which is atomistically defined as a function of the fraction of atoms occupying the correct lattice sites (e.g., the face-center positions) and the fraction of such sites in the lattice. However, the S of a real sample cannot be experimentally determined directly from this definition since the number of atoms occupying a particular lattice site is not accessible. There are two options for the experimental determination of S:[27] (i) comparing the integrated intensity of a superlattice and a fundamental line in the experimental powder diffraction pattern of the sample (let us call this S_{int}) and (ii) evaluating the extent of tetragonality of the $L1_0$ crystals by assuming a model that relates the c/a ratio to the degree of order (let us call this S_{tetr}). The two approaches have been directly compared in Ref. 30 or can be compared from the data reported in studies about other alloys (FePt and CoPt) with $L1_0$ ordering.[31] The comparison shows that (i) for the same sample, the two approaches give different values of S, with S_{tetr} being always larger than S_{int}, and (ii) the relative difference decreases as S increases. One reason of this can be found in the fact that, while the c/a ratio is deduced from the peak positions and, hence, does not depend on the relative proportion of the ordered and disordered phases, the intensity ratio between superlattice and fundamental lines depends both on the ordering degree of the crystals and on the amount of the ordered phase formed. In the choice of the intensity ratio as an indicator of the degree of long-range order of an alloy, one has to assume that the order–disorder transformation occurs continuously and homogeneously throughout the alloy, meaning that it starts with a small order parameter in all the grains composing the sample and the order gradually builds up with the time (or temperature) of annealing. By contrast, other mechanisms of ordering can be observed, especially in films grown close to room temperature, namely, the discontinuous (or inhomogeneous) transformation, occurring by the nucleation and growth of ordered domains along grain boundaries.[32–34] In this case, especially in the early stages of the transformation, the sample is composed of a mixture of ordered and disordered grains, and the degree of the long-range order of the chemically ordered regions (i.e., the $L1_0$ phase) can be better described by S_{tetr}. In the latter case, the volume average of the order parameter has to be taken into account, which is $S_{alloy} = f_v\ S_{tetr}$. The volume fraction of the ordered phase formed (transformed fraction), which is

$$f_v = \frac{V_{L1_0}}{V_{sample}}, \tag{3}$$

can be calculated from XRD data as a product of S_{tetr} and the intensity ratio between superlattice and fundamental lines,[35]

$$f_v = \frac{1}{S_{tetr}^2} \frac{\left(\frac{I_s}{I_f}\right)_{meas}}{\left(\frac{I_s}{I_f}\right)_{calc}}, \tag{4}$$

where I_s is the integrated intensity of a superlattice peak and I_f the integrated intensity of a fundamental peak, and S_{tetr} is the previously defined order parameter. Subscript *meas* indicates the experimentally measured intensities, while *calc* denotes the intensities calculated from the intensity equation for a diffraction peak,[36]

$$I = |F^2| m L_p(\theta) T(\theta), \tag{5}$$

where F is the structure factor, m is the multiplicity factor, and $L_p(\theta)$ and $T(\theta)$ are the Lorenz–polarization factor and the temperature factor, respectively, dependent on the Bragg angle θ. This factorization allows us to take into account both the incomplete ordering of the $L1_0$ phase and the increase in the amount of this phase occurring during a discontinuous transformation.

From the x-ray diffractograms of the annealed samples, we have, therefore, chosen the fundamental (111) and the superlattice (110) peaks in order to determine the volume fraction: the (111) peak was fitter with a Pseudo–Voigt type function, i.e., a linear combination of a Lorentzian $L(2\theta, H)$ and a Gaussian $G(2\theta,H)$, whereas the superlattice (110) peak was fitted with a Gaussian function. These peaks have good statistics compared with the peak (200) and give a better fit. The fittings were performed with the Fityk software (version 0.9.8).[37]

Since it is assumed that after 120 min of annealing, the phase transformation is complete ($f_v = 1$, $S_{tetr} = 1$), from Eq. (4), it follows that, at this annealing time,

$$\left(\frac{I_s}{I_f}\right)_{meas,120\ min} = \left(\frac{I_s}{I_f}\right)_{calc,120\ min}. \tag{6}$$

Thus, the transformed fraction of the $L1_0$ phase at each annealing time t, denoted by $f_v(t)$, can be written as

$$f_v(t) = \frac{1}{S_{tetr,\,t}^2} \frac{\left(\frac{I_s}{I_f}\right)_{meas,t}}{\left(\frac{I_s}{I_f}\right)_{meas,120\ min}}. \tag{7}$$

The values of the transformed fraction are given in Table II.

B. From magnetic properties

The transformed phase fraction can also be calculated from the hysteresis loop data, in an independent way, using the following expression:[38]

$$H_c = f_v^{soft} H_c^{soft} + f_v^{hard} H_c^{hard}, \tag{8}$$

where H_c^{soft} (H_c^{hard}) and f_v^{soft} (f_v^{hard}) are the coercive field and the volume fraction of the soft (hard) phase, respectively. It is important to remark that Eq. (8) considers the two soft and hard phases magnetically decoupled. In the case of the studied disorder → order phase transformation, Eq. (8) can be written as

$$H_c(t) = H_c^{fcc} + (H_c^{L1_0} - H_c^{fcc}) f_v^{L1_0}(t), \tag{9}$$

with $f_v^{fcc}(t) + f_v^{L1_0}(t) = 1$.

TABLE II. Coercive field H_c and transformed fraction obtained by XRD data f_v^{XRD} and by AGFM data f_v^{AGFM}, with their average value $f_v^{average}$.

Time (min)	0	1	2	5	10	20	30	40	50	60	120
H_c (Oe)	5	616	925	1176	1340	1552	1710	1819	1907	1973	2113
f_v^{XRD}	0	0.526	0.648	0.798	0.819	0.804	0.921	0.974	0.932	1.029	1.000
f_v^{AGFM}	0	0.290	0.437	0.555	0.634	0.734	0.809	0.861	0.903	0.934	1.000
$f_v^{average}$	0	0.408	0.542	0.676	0.726	0.769	0.865	0.917	0.917	0.981	1.000

From Eq. (9), we finally deduce the transformed fraction of the $L1_0$ phase,

$$f_v^{AGFM}(t) = f_v^{L1_0}(t) = \frac{H_c(t) - H_c^{fcc}}{H_c^{L1_0} - H_c^{fcc}}, \tag{10}$$

where H_c^{fcc} is the coercive field of the disordered FePd phase, obtained from the hysteresis loop of the as-prepared sample (5 Oe, as discussed previously), and $H_c^{L1_0}$ is the coercive field of the ordered $L1_0$ FePd phase, taken from the sample where the transformation is complete after annealing at 550 °C for 120 min (and, therefore, 2113 Oe). The values of the transformed fraction of the $L1_0$ ordered phase as a function of the annealing time are given in Table II.

Figure 4 shows the transformed fraction of the $L1_0$ phase as a function of the annealing time obtained with the two independent methods, using the values reported in Table II. As can be clearly seen, the results are in very good agreement. It is worth remarking that f_v has been determined exploiting only rather common experimental techniques, instead of the much more complex and expensive TEM and Mössbauer spectrometry investigations usually required for such purposes.[2,13]

This result allows us to correlate the coercive field of the samples annealed for different times to their respective transformed volume fractions, as shown in Fig. 5, which exhibits a remarkable linear dependence of the two quantities, as also already observed in Refs. 2 and 13. In Fig. 5, an average value for the transformed fraction, obtained from the two techniques, is used.

It is worth underlining that transformed fraction values obtained with the two techniques, although remarkably in agreement, are not coincident, as x-ray diffraction and magnetometry are two extremely different techniques, investigating very different aspects of the samples. From their similar behavior, one can infer that the processes of phase transformation can be studied, with comparable results, both from structural and magnetic measurements. If other techniques were available for studying the same phenomena, it is expected that they would provide similar results,

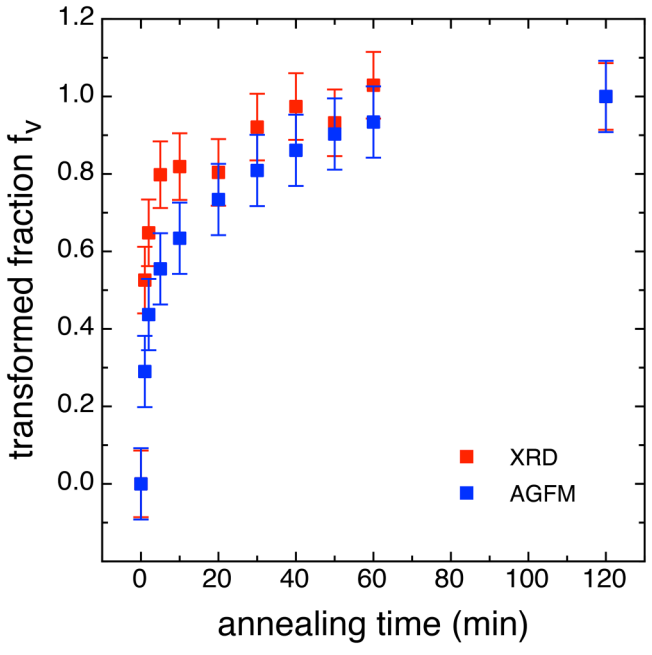

FIG. 4. $L1_0$ transformed fraction obtained by XRD and AGFM as a function of the annealing time.

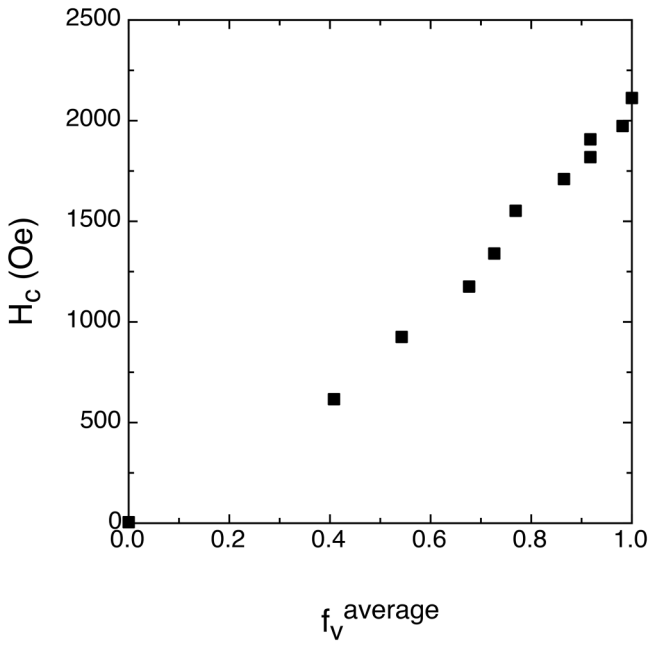

FIG. 5. Coercive field as a function of the average transformed volume fraction.

and discrepancies, if any, can be attributed to the details of the experimental techniques that are very different from those of the numerous samples.

From these results, we can, therefore, assume that Eq. (10) is valid in the generalized case of disordered → ordered phase transformations, with uncoupled phases, allowing the determination of the transformed fraction of the ordered phase.

C. Order parameter of the alloy

The order parameter of the alloy as a whole, S_{alloy}, can now be calculated with the following expression:[34,39]

$$S_{alloy} = S_{tetr} f_v^{average}, \tag{11}$$

where S_{tetr} and $f_v^{average}$ values can be found in Tables I and II. Its evolution as a function of the annealing time is reported in Fig. 6. After approximately 10 min of annealing, S_{tetr} becomes equal to 1, whereas the ordering parameter of the alloy is still lower than unity. This is due to the progressive growth of the average volume fraction f_v of the ordered $L1_0$ phase in the alloy, indicating that for certain annealing times, the disordered fcc and ordered $L1_0$ phases coexist. The transformation of the former into the latter is a first order transition. It is worth remarking that, as already discussed for Fig. 2(a), an order parameter close to 1 at long annealing times ensures that a well-developed $L1_0$ phase is present, but the anisotropy axes of the $L1_0$ crystals are oriented in space in a disordered way, which does not give rise to a dominant perpendicular anisotropy.

It is now possible to correlate the evolution with the annealing time of the coercive field and of the average order parameter of the $Fe_{56}Pd_{44}$ alloy, as shown in Fig. 7.

The use of S_{alloy} as the order parameter against which the coercivity values should be analyzed is in agreement with that of Ref. 2, which suggests that a microstructural factor relating to the ordered volume fraction and that scales similarly to it should be taken into account. The linear relationship between H_c and S_{alloy} shown in Fig. 7 supports this choice.

The linear relationship shown in Fig. 7 can be written as follows:

$$H_c(t) = \frac{H_c^{L1_0} - H_c^{fcc}}{S_{L1_0}} S_{alloy}(t) + H_c^{fcc}. \tag{12}$$

It is worth remarking that the theoretical line calculated with Eq. (12) is completely determined by available experimental data and is not the result of a fitting procedure. It is also in very good agreement with the experimental values. An almost linear relationship between the coercive field and the mean order parameter of the alloy is, therefore, clearly highlighted.

V. KINETICS OF GRAIN GROWTH AND PHASE TRANSFORMATION

A. Kinetics of grain growth

The kinetics of the transformation of the disordered fcc phase into the ordered $L1_0$ one, in the studied polycrystalline $Fe_{56}Pd_{44}$

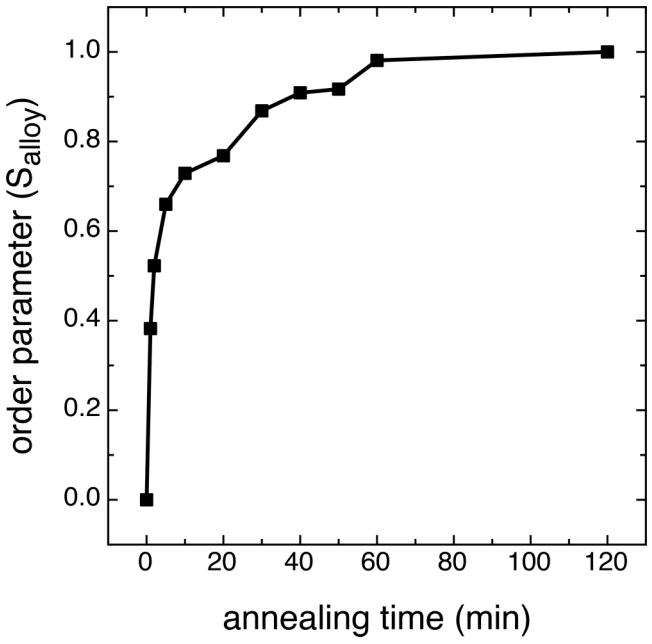

FIG. 6. S_{alloy} order parameter of the alloy $Fe_{56}Pd_{44}$ as a function of the annealing time.

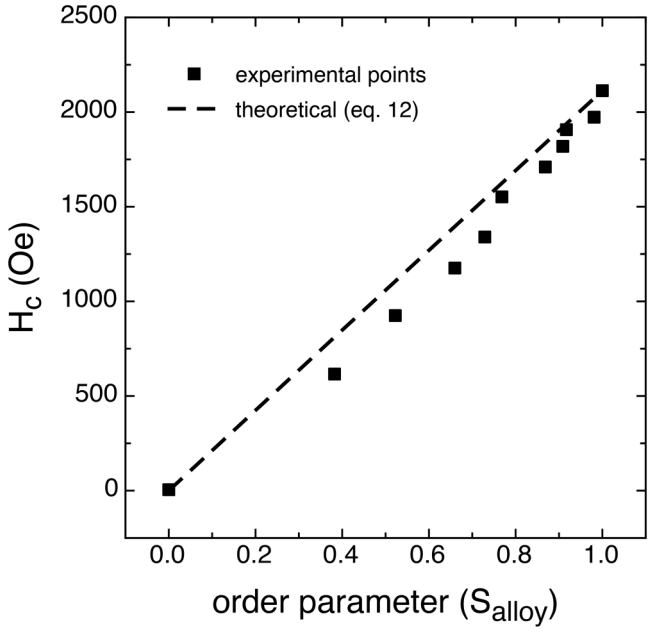

FIG. 7. Coercive field H_c as a function of S_{alloy} order parameter of the alloy $Fe_{56}Pd_{44}$. The line results from Eq. (12).

thin films, can be followed by examining the evolution of the grain size as a function of the annealing time. The crystallite size <D> calculated from XRD data and reported in Table I is plotted in Fig. 8 as a function of the annealing time. It can be clearly seen that the size of the grains varies slowly with the annealing time. Indeed, the evolution of grain growth is described by the normal grain growth equation, which is expressed as[14,40,41]

$$D^n - D_0^n = ct, \tag{13}$$

where n is the grain growth exponent, D_0 is the initial grain size, and c is the growth rate, that is given by the following expression: $c = c_0 \exp(-E_a/k_BT)$, where E_a is the activation energy for grain growth, T is the temperature, and k_B is the Boltzmann constant. To determine the parameters c and n for our thin film sample, the experimental data of Fig. 8 have been fitted with Eq. (13), obtaining $c = 1.45 \times 10^8$ nm$^{8.24}$/min and $n = 8.24$.

Such a value of the grain growth exponent is compatible with similar findings in the literature either for FePd or for FePt systems: values in the 8–11 range are specific for slow grain growth rates,[14,42] whereas smaller values, in the 3–4 range, are associated with much faster grow rates.[31,42] During the grain growth process, a disordered alloy undergoes microstructure changes through a combination of two processes, i.e., the ordering of the atoms in the alloy, and the recrystallization of the grains. The latter develops through the nucleation of new grains and through their growth. In fact, in our case, the evolution of grain size as a function of annealing time (Fig. 8) can be divided into two main parts corresponding to different microstructures. In the first part, approximately up to 20 min of annealing time, the grain size increases from 10 to 14 nm. Beyond 20 min, in the second part, the variation of the grain size is approximately equivalent (up to ∼4 nm), but it takes place over a much longer annealing time interval. This difference is due to the high density of defects, particularly, the grain boundaries, in the as-deposited film, which create a significant driving force contributing to nucleation as well as ordering. This phenomenon leads to the phase transformation of the fcc structure phase toward the tetragonal structure $L1_0$ in the $Fe_{56}Pd_{44}$ alloy. Indeed, during this interval of time, the density of the grain boundaries decreases in the $Fe_{56}Pd_{44}$ alloy. At $t = 20$ min, the alloy reaches a transformed fraction of 76.9% (see Table II) and an average order parameter S_{alloy} of 0.769. From this instant of time, new kinds of defects will be created in the ordered alloy, such as antiphase walls, twins, and polytwins, leading to a different kinetics.[9]

Furthermore, as depicted in Fig. 8, the shape of the curve indicates that the growth of grain as a function of time is a continuous process. The same shape of the curve was obtained for FePt thin films.[14,43] However, this continuous process takes place according to different mechanisms, where the reduction of grain boundaries (associated with the initial grain growth) is at a certain instant of time suppressed and is followed by the development of new microstructure defects. Several mechanisms responsible for the suppression of grain growth have been suggested in the literature, such as the presence of a second phase that induces the trapping of the movement of the grain boundaries,[44] the appearance of grain boundaries etching on the surface of the thin film,[45] or the correlation between adjacent grains that accelerates the stagnation of grain growth.[46] All these mechanisms can, in principle, induce the slowdown of the grain growth process in our samples.

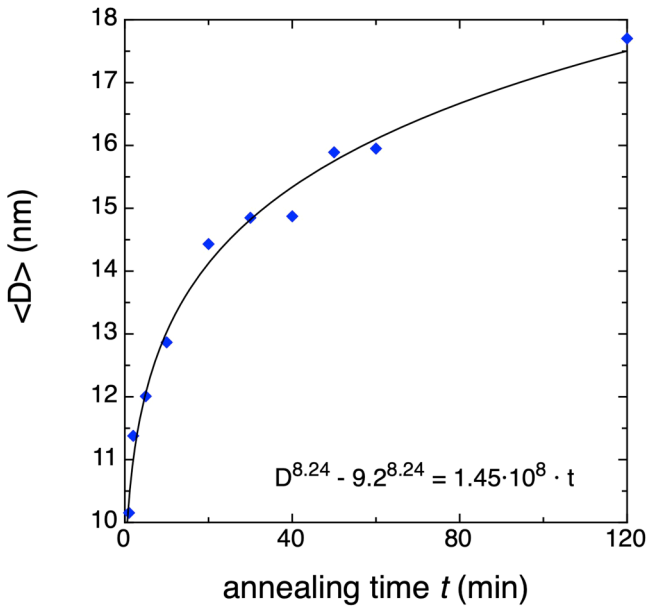

FIG. 8. Grain size as a function of the annealing time (symbols), fitted with Eq. (13) (line).

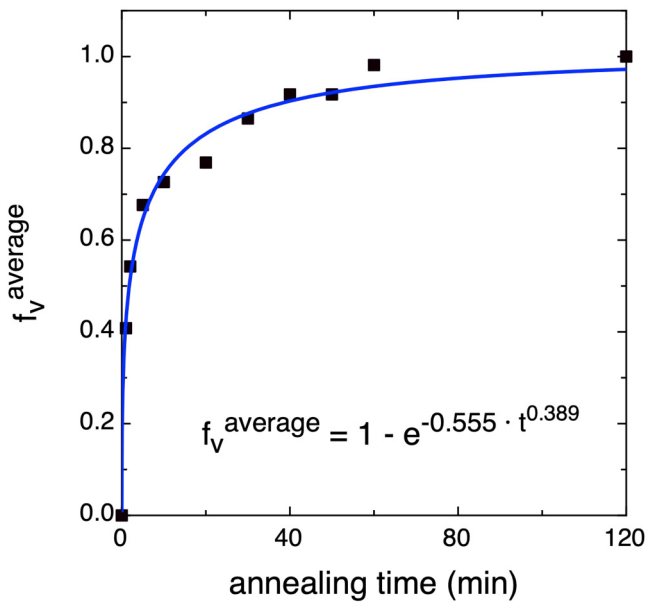

FIG. 9. Transformed volume fraction as a function of the annealing time (symbols) and fitting with Eq. (14) (line).

TABLE III. Theoretical values of Avrami exponent n_A.[48]

Growth mechanism	Nucleation mechanism	Dimensionality growth		
		1D	2D	3D
Interface-controlled growth	Constant nucleation rate	$n_A = 2$	$n_A = 3$	$n_A = 4$
	Instantaneous nucleation	$n_A = 1$	$n_A = 2$	$n_A = 3$
	Decreasing nucleation rate	$n_A = 1–2$	$n_A = 2–3$	$n_A = 3–4$
Diffusion-controlled growth	Constant nucleation rate	$n_A = 1.5$	$n_A = 2$	$n_A = 2.5$
	Instantaneous nucleation	$n_A = 0.5$	$n_A = 1$	$n_A = 1.5$
	Decreasing nucleation rate	$n_A = 0.5–1.5$	$n_A = 1–2$	$n_A = 1.5–2.5$

B. Kinetics of $A1 \rightarrow L1_0$ phase transformation

The Johnson–Mehl–Avrami–Kolmogorov (JMAK) theory has been used to study the kinetics of the phase transformation from the disordered $A1$ phase to the ordered $L1_0$ phase. This theory is based on the nucleation and growth mechanisms, where the nucleation sites are randomly distributed to form grains. Thus, the concept of nucleation-growth transformation can be expressed using the evolution of the transformed fraction $f_v(t)$ of the ordered phase as a function of the annealing time:[12]

$$f_v^{average}(t) = 1 - e^{-kt^{n_A}}, \tag{14}$$

where k is the overall rate constant that depends on temperature and the index n_A is the exponent of Avrami that includes contributions from growth and nucleation as well as the dimensionality of growth (i.e., 1D, 2D, or 3D).

Figure 9 reports the average values of the transformed fraction $f_v^{average}$ as a function of the annealing time, together with the fit exploiting Eq. (14) using k and n_A as free parameters.

The fit gave $n_A = 0.39 \pm 0.03$ and $k = 0.555\ \text{min}^{-n_A}$. The quality of the fitting shows that Avrami law is quite well followed by the experimental data.

The Avrami exponent n_A of Eq. (14) describes the kinetics of transformation of the $A1$ phase into the $L1_0$ and can be expressed as the sum of two terms: a nucleation condition term (a), and the one related to the growth process, combining the growth dimensionality (b) and the growth mechanism (c): $n_A = a + b * c$.[47] The nucleation process has three different modes: (1) continuous, where the nucleation speed does not vary with time (i.e., the nucleation rate is constant) and a takes the value of 1; (2) instantaneous, where site saturation occurs and a takes the value of 0; and (3) with decreasing speed over time. The effect of the growth process on the Avrami exponent is factorized in order to take into account the possible combinations of the growth mechanism ($c = 0.5$ for diffusion-controlled growth and $c = 1$ for interface-controlled growth) and the dimensionality of the growth in space (b = 1D, 2D, or 3D). The different possible combinations of the Avrami exponent are summarized in Table III.[48]

In our case, the Avrami exponent $n_A \sim 0.4$ that we obtained for our FePd system indicates that the $A1 \rightarrow L1_0$ phase transformation is diffusion controlled, is one-dimensional (1D), and proceeds with the nucleation rate decreasing with time. Values of the same order of magnitude (0.3) have been obtained for FePt systems,[13,34] where heterogeneous nucleation mechanisms have been invoked. Such values smaller than 1 are typical of thin film systems, whereas bulk alloys are characterized by Avrami exponent values between 2 and 4.[49]

We can, therefore, summarize the evolution of the microstructure of our $Fe_{56}Pd_{44}$ thin films upon heating: the fcc disordered phase initially present gradually transforms into the ordered $L1_0$ one by means of an inhomogeneous process involving both nucleation and growth of new grains of the ordered phase in the fcc matric and its progressive ordering. After 10 min of annealing, the ordering transformation is complete, as demonstrated by the ordering parameter S_{tetr} of the $L1_0$ phase (see Table I), but the volume fraction of the transformed phase is still sensibly lower than unity, reaching a value close to 1 only after 60 min of annealing (see Fig. 9). Mössbauer investigations[9] revealed that in these films, antiphase boundaries and twin boundaries develop. As the activation energy of the lattice diffusion and of the disorder–order transformation for alloys with $L1_0$ atomic ordering are typically of the same order of magnitude (see, e.g.,[42,43] for a comparison), and since the antiphase domains growth is due to the diffusion of vacancies at the antiphase boundaries,[49] we can infer that the order–disorder transformation in the $Fe_{56}Pd_{44}$ alloy is mainly due to the role of vacancies. Their diffusion at the grain boundaries and at antiphase boundaries induces grain size growth, which is in agreement with the results in Fig. 8.

VI. CONCLUSIONS

(1) The evolution of the grain size as a function of the annealing time obeys the law of normal grain growth $D^n - D_0^n = ct$, where n is the growth exponent equal to 8.24. Correspondingly, the average grain sizes $\langle D \rangle$ are smaller than the critical grain size D_{MD} for multi-domain FePd particles ($D_{MD} = 40$ nm) even after prolonged annealing (120 min). This result indicates that although the $Fe_{56}Pd_{44}$ thin films alloy is characterized by a high density of defects, the growth of the grains is slow. Some defects, such as grain boundaries, were developed during processing, while others, such as twinned domains, twin boundaries, and antiphase boundaries, were developed during heat treatment.

(2) The volume fraction of the transformed $L1_0$ phase has been calculated using the following expression:

$$f_v^{L1_0}(t) = \frac{H_c(t) - H_c^{fcc}}{H_c^{L1_0} - H_c^{fcc}}, \tag{15}$$

which we propose as valid in the generalized case of disordered → ordered phase transformations, allowing the determination of the transformed fraction of the ordered phase from purely magnetic measurements.

(3) We examined the kinetics of the $A1 \rightarrow L1_0$ transformation in the $Fe_{56}Pd_{44}$ alloy annealed at 550 °C for up to 120 min. We found that the transformation obeys Avrami's law $f_v(t) = 1 - \exp(-kt^{n_A})$, where f_v is the transformed volume fraction. The obtained Avrami exponent is equal to $n_A \sim 0.4$. This value indicates that the phase transformation is controlled by the nucleation mechanism, with a decreasing nucleation rate, which is a consequence of rapid transformation. The low value of the Avrami exponent is due to the presence of structural defects.

(4) An almost linear relationship between the coercive field and the average order parameter of the alloy has been established: $H_c(t) = \frac{H_c^{L1_0} - H_c^{fcc}}{S_{L1_0}} S_{alloy}(t) + H_c^{fcc}$.

The evolution of the coercivity with the annealing time obtained through this formula is determined exclusively from available experimental data and is in rather good agreement with the measured coercivity values. An almost linear relationship between the coercive field and the average order parameter of the alloy is, therefore, clearly highlighted.

ACKNOWLEDGMENTS

This work has been partially performed at NanoFacility Piemonte, an INRIM Laboratory supported by the Compagnia di San Paolo Foundation.

AUTHOR DECLARATIONS

Conflict of Interest

The authors have no conflicts to disclose.

DATA AVAILABILITY

The data that support the findings of this study are available from the corresponding author upon reasonable request.

REFERENCES

[1]D. Weller, A. Moser, L. Folks, M. E. Best, W. Lee, M. F. Toney, M. Schwickert, J.-U. Thiele, and M. F. Doerner, "High K/sub u/materials approach to 100 Gbits/in^2," IEEE Trans. Magn. **36**, 10–15 (2000).

[2]R. A. Ristau, K. Barmak, L. H. Lewis, K. R. Coffey, and J. K. Howard, "On the relationship of high coercivity and $L1_0$ ordered phase in CoPt and FePt thin films," J. Appl. Phys. **86**, 4527 (1999).

[3]T. Klemmer, D. Hoydick, H. Okumura, B. Zhang, and W. A. Soffa, "Magnetic hardening and coercivity mechanisms in $L1_0$ ordered FePd ferromagnets," Scr. Metall. Mater. **33**, 1793 (1995).

[4]B. Zhang and W. A. Soffa, "Magnetic domains and coercivity in polytwinned ferromagnets," Phys. Status Solidi A **131**, 707–725 (1992).

[5]D. Halley, B. Gilles, P. Bayle-Guillemaud, R. Arenal, A. Marty, G. Patrat, and Y. Samson, "Chemical ordering in magnetic FePd/Pd (001) epitaxial thin films induced by annealing," Phys. Rev. B **70**, 174437 (2004).

[6]C. H. Hsiao, Y. D. Yao, S. C. Lo, H. W. Chang, and C. Ouyang, "Domain wall pinning on strain relaxation defects (stacking faults)in nanoscale FePd (001)/MgO thin films," Appl. Phys. Lett. **107**, 142407 (2015).

[7]A. Kovács, K. Sato, and Y. Hirotsu, "High-resolution transmission electron microscopy analysis of $L1_0$ ordering process in Fe/Pd thin layers," J. Appl. Phys. **102**, 123512 (2007).

[8]E. T. Moiseenko, R. R. Altunin, and S. M. Zharkov, "Formation of the atomically ordered $L1_0$ structure with the [001] orientation during the solid-state reaction in Fe/Pd bilayer thin films," Phys. Solid State **59**, 1233–1237 (2017).

[9]S. Bahamida, A. Fnidiki, M. Coisson, G. Barrera, F. Celegato, E. S. Olivetti, P. Tiberto, A. Laggoun, and M. Boudissa, "Effect of the $A1$ to $L1_0$ transformation on the structure and magnetic properties of polycrystalline $Fe_{56}Pd_{44}$ alloy thin films produced by thermal evaporation technique," Thin Solid Films **668**, 9–13 (2018).

[10]J. R. Skuza, C. Clavero, K. Yang, B. Wincheski, and R. A. Lukaszew, "Microstructural, magnetic anisotropy, and magnetic domain structure correlations in epitaxial FePd thin films with perpendicular magnetic anisotropy," IEEE Trans. Magn. **46**, 1886–1889 (2010).

[11]Y. C. Chang, S. N. Hsiao, S. H. Liu, S. K. Chen, Y. T. Liu, H. Y. Lee, A. C. Sun, and J. G. Dhu, "Influence of stoichiometry and growth temperature on the crystal structure and magnetic properties of epitaxial $L1_0$ Fe-Pd (001) films," J. Appl. Phys. **115**, 17A740 (2014).

[12]M. Avrami, "Kinetics of phase change. I. General theory," J. Chem. Phys. **7**, 1103–1112 (1939).

[13]F. E. Spada, F. T. Parker, C. L. Platt, and J. K. Howard, "X-ray diffraction and Mössbauer studies of structural changes and $L1_0$ ordering kinetics during annealing of polycrystalline $Fe_{51}Pt_{49}$ thin films," J. Appl. Phys. **94**, 5123–5134 (2003).

[14]N. Zotov, R. Hiergeist, A. Savan, and A. Ludwig, "Effects of annealing time on the structural and magnetic properties of $L1_0$ FePt thin films," Thin Solid Films **518**, 4977–4985 (2010).

[15]B. Lacroix, "Influence des défauts cristallins sur les changements de phase induits par faisceaux d'ions dans les films minces d'oxyde d'yttrium Y_2O_3," Thèse de doctorat (Université de Poitiers, 2006), available at http://theses.univ-poitiers.fr/notice/view/2162.

[16]D. C. Berry and K. Barmak, "Time-temperature-transformation diagrams for the $A1$ to $L1_0$ phase transformation in FePt and FeCuPt thin films," J. Appl. Phys. **101**, 014905 (2007).

[17]R. H. Yu, S. Basu, Y. Zhang, A. Parvizi-Majidi, and J. Q. Xiao, "Pinning effect of the grain boundaries on magnetic domain wall in FeCo-based magnetic alloys," J. Appl. Phys. **85**, 6655–6659 (1999).

[18]G. Herzer, "Soft magnetic nanocrystalline materials," Scr. Metall. Mater. **33**, 1741–1756 (1995).

[19]K. Suzuki, G. Herzer, and J. M. Cadogan, "The effect of coherent uniaxial anisotropies on the grain-size dependence of coercivity in nanocrystalline soft magnetic alloys," J. Magn. Magn. Mater. **177**, 949–950 (1998).

[20]E. F. Kneller and F. E. Luborsky, "Particle size dependence of coercivity and remanence of single-domain particles," J. Appl. Phys. **34**, 656–658 (1963).

[21]V. Gehanno, "Anisotropie magnétique perpendiculaire des couches minces épitaxiées d'alliage ordonnes FePd," Ph.D. thesis (University Joseph-Fourier, 1997).

[22]C. Clavero, J. M. García-Martín, J. L. Costa Kramer, G. Aremelles, A. Cebollada, Y. Huttel, R. A. Lukaszew, and A. J. Kellock, "Temperature and thickness dependence at the onset of perpendicular magnetic anisotropy in FePd thin films sputtered on MgO(001)," Phys. Rev. B **73**, 174405 (2006).

[23]F. M. Takata, G. Pattanaik, W. A. Soffa, P. T. A. Sumodjo, and G. Zangari, "Synthesis of $L1_0$ Fe-Pd films by electrodeposition and thermal annealing," Electrochem. Commun. **10**, 568 (2008).

[24]S. Bahamida, A. Fnidiki, M. Coïsson, A. Laggoun, G. Barrera, F. Celegato, and P. Tiberto, "Mixed exchange-coupled soft α-($Fe_{80}Fe_{20}$) and hard $L1_0$FePd phases in $Fe_{64}Pd_{36}$ thin films studied by first order reversal curves," Mater. Sci. Eng. B **226**, 47 (2017).

[25]B. W. Roberts, "X-ray measurement of order in CuAu," Acta Metall. **2**(4), 597–603 (1954).

[26]P. S. Rudman and B. L. Averbach, "X-ray determinations of order and atomic sizes in Co-Pt solid solutions," Acta Metall. **5**(2), 65–73 (1957).

[27]S. Bahamida, A. Fnidiki, A. Laggoun, and A. Guittoum, "A comparative structural and magnetic study of $Fe_{100-x}Pd_x$ ($x = 15$, 20 and 36) thin films deposited on Si(100) and glass substrates," J. Magn. Magn. Mater. **392**, 139–147 (2015).
[28]Y. Tamada, Y. Morimoto, S. Yamamoto, M. Takano, S. Nasu, and T. Ono, "Effects of annealing time on structural and magnetic properties of $L1_0$-FePt nanoparticles synthesized by the SiO_2-nanoreactor method," J. Magn. Magn. Mater. **310**, 2381–2383 (2007).
[29]J. A. Christodoulides, P. Farber, M. Dannl, H. Okumura, G. C. Hadjipanaysi, V. Skumryev, A. Simopoulos, and D. Weller, IEEE Trans. Magn. **37**, 1292–1294 (2001).
[30]K. Barmak, J. Kim, L. H. Lewis, K. R. Coffey, M. F. Toney, A. J. Kellock, and J.-U. Thiele, "On the relationship of magnetocrystalline anisotropy and stoichiometry in epitaxial $L1_0$ CoPt (001) and FePt (001) thin films," J. Appl. Phys. **98**(3), 033904 (2005).
[31]D. E. Laughlin, K. Srinivasan, M. Tanase, and L. Wang, "Crystallographic aspects of $L1_0$ magnetic materials," Scr. Mater. **53**(4), 383–388 (2005).
[32]M. Rajkovic and R. A. Buckley, "Ordering transformations in Fe-50Co based alloys," Met. Sci. **15**(1), 21–29 (1981).
[33]A. Cebollada, R. F. C. Farrow, and M. F. Toney, in *Magnetic Nanoestructures*, edited by H. S. Nalwa (American Scientific, Los Angeles, 2002), pp. 93–122.
[34]K. Tanaka, T. Ichitsubo, M. Amano, M. Koiwa, and K. Watanabe, "Formation of mono-variant $L1_0$ structure on ordering of FePd under magnetic fields," Mat. Trans. JIM **41**, 917–922 (2000).
[35]B. D. Cullity, "Elements of x-ray diffraction," in *Addison-Wesley Series in Metallurgy and Materials*, 2nd ed. (Addison-Wesley Pub. Co, Reading, MA, 1978).
[36]See https://fityk.nieto.pl for Fityk software features and download.
[37]F. Liu, Y. Hou, and S. Gao, "Exchange-coupled nanocomposites: Chemical synthesis, characterization and applications," Chem. Soc. Rev. **43**, 8098–8113 (2014).
[38]C. B. Ndao, "Matériaux magnétiques en couches.: Etudes des systèmes FePt et FeRh," Thèse de doctorat (Université de Grenoble, 2011).
[39]H. V. Atkinson, "Overview no. 65: Theories of normal grain growth in pure single-phase systems," Acta Metall. **36**, 469–491 (1988).
[40]C. V. Thompson, "Grain growth in thin films," Annu. Rev. Mater. Sci. **20**, 245–268 (1990).
[41]N. Zotov, J. Feydt, and A. Ludwig, "Dependence of grain sizes and microstrains on annealing temperature in Fe/Pt multilayers and $L1_0$ FePt thin films," Thin Solid Films **517**, 531–537 (2008).
[42]M. Watanabe, T. Nakayama, K. Watanabe, T. Hirayama, and A. Tonomura, "Microstructure and magnetic properties of high-coercive Fe-Pt alloy thin films," Mater. Trans. JIM **37**, 489–493 (1996).
[43]S. P. Riege, C. V. Thompson, and H. J. Frost, "Simulation of the influence of particles on grain structure evolution in two-dimensional systems and thin films," Acta Mater. **47**, 1879–1887 (1999).
[44]H. J. Frost, C. V. Thompson, and D. T. Walton, "Simulation of thin film grain structures—I. Grain growth stagnation," Acta Mater. **38**, 1455–1462 (1990).
[45]C. Lou and M. A. Player, "Advection-diffusion model for the stagnation of normal grain growth in thin films," J. Phys. D: Appl. Phys. **35**, 1805–1811 (2002).
[46]N. Bordeaux, A. M. Montes-Arango, J. Liu, K. Barmak, and L. H. Lewis, "Thermodynamic and kinetic parameters of the chemical order-disorder transformation in $L1_0$ FeNi (tetrataenite)," Acta Mater. **103**, 608–615 (2016).
[47]S. C. Liou and S. Y. Chen, "Transformation mechanism of different chemically precipitated apatitic precursors into β-tricalcium phosphate upon calcinations," Biomaterials **23**, 4541 (2002).
[48]X. H. Li, B. T. Liu, W. Li, H. Y. Sun, D. Q. Wu, and X. Y. Zhang, "Atomic ordering kinetics of FePt thin films: Nucleation and growth of $L1_0$ ordered domains," J. Appl. Phys. **101**, 093911(1)–093911(5) (2007).
[49]M. Porta, C. Frontera, E. Vives, and E. T. Castán, "Effect of the vacancy interaction on antiphase domain growth in a two-dimensional binary alloy," Phys. Rev. B **56**, 5261 (1997).